Earth System
Open Access
Science
Data
Discussions

1 Introduction

Extensive ice-penetrating radar data has been collected over the years in the Dome C region of the East Antarctic Plateau. These data were initially collected to characterize the Dome C ice core site. Subsequently, the Dome C region was revealed as one of the promising regions to have retained million-year-old ice, based on modeling thermodynamic results (Van Liefferinge and Pattyn, 2013; Fischer et al., 2013; Van Liefferinge et al., 2018). The rare combination of thick ice, relatively low snow accumulation rate, low geothermal heat flux, slow ice flow and clear undisturbed englacial stratigraphy made this site one of the primary target drilling sites for the Beyond EPICA - Oldest Ice European project (BE-OI), with the added advantage of its proximity to the Concordia station for logistics. Providing detailed constraints on the ice sheet in this region including its internal age structure and its temporal flow stability motivated the extensive tracing of internal stratigraphy over the entire Dome C region. All published radar data sets available at the time in this region were used to construct the internal stratigraphy presented here.

Ice-penetrating radar became the prime method to image the hidden bedrock beneath the ice and derive ice thickness in the 1960s (Robin et al., 1969). By the 1970s, the internal stratigraphy of the ice column started being examined including the origin of the internal reflecting horizons (IRHs) (Clough, 1977). IRHs can have three possible origins: (1) density changes, typically restricted to the firn column, (2) ice chemical composition variation, resulting from the successive deposition and burial of aerosols and dust particles on the ice and/or (3) ice fabrics (Clough, 1977; Millar, 1981; Fujita and Mae, 1994; Siegert et al., 1998b; Fujita et al., 1999), usually most strongly observed at depth or in areas of shear flow. The IRH presented in this data set are thought to be dominated by ice chemistry variations, considering their relative depths and the relative flow stability of this part of the ice sheet. Such IRHs are generally assumed to be isochronous (Whillans, 1976; Siegert et al., 1998a) and, as a result, can be used as time markers and thus provide a dated stratigraphy as long as they are laterally continuous (Siegert, 1999; Fujita et al., 1999). Ages are generally assigned to the IRHs where the radar transects pass close to an ice core site, sometimes requiring some assumptions about how to interpolate between the point of closest approach and the ice core site (Siegert et al., 1998a; Cavitte et al., 2016; Winter et al., 2015). IRHs have also been used extensively to characterize past and present flow conditions (Jacobel et al., 1993; Siegert et al., 2004; Dahl-Jensen et al., 2013; Bingham et al., 2015; Kingslake et al., 2016; Beem et al., 2018), provide constraints in the reconstruction of past accumulation rates (Eisen et al., 2008; Casey et al., 2014; Koutnik et al., 2016), estimate englacial temperature (Matsuoka, 2011; MacGregor et al., 2012), measure basal reflectivity and thus reveal subglacial hydrological drainage (Carter et al., 2007, 2009; Schroeder et al., 2015; Siegert et al., 2016) (see Schroeder et al., 2020, for more applications).

While an extensive internal stratigraphic data set has already been obtained for the Greenland Ice Sheet (MacGregor et al., 2015), in Antarctica, due to its sheer size, it will require more time and the acquisition of additional ice-penetrating radar data in order to: (1) connect existing surveys and (2) extend coverage to under-surveyed parts of the ice sheet. The SCAR AntArchitecture project was commissioned for this specific purpose. The construction of a comprehensive Antarctic-wide IRH data set will both play a key role for projects such as the Beyond EPICA - Oldest Ice European search for million-year-old ice (Van Liefferinge and Pattyn, 2013; Parrenin et al., 2017) and provide valuable additional constraints to inverse models,

Number: 1 Author: oeisen   Subject: Hervorheben   Date: 29.01.21, 08:22:52
at the time

Number: 2 Author: oeisen   Subject: Hervorheben   Date: 29.01.21, 08:23:03
conductivity

Number: 3 Author: oeisen   Subject: Hervorheben   Date: 29.01.21, 08:26:04
reference to report

45   potentially reducing the lack of unique solutions, a persistent problem until now (Morse et al., 1998; Eisen et al., 2008; Koutnik et al., 2016; Parrenin et al., 2017; Muldoon, 2018), as well as solving the problem of modeling 3D data in simple 1-D or 2-D models (Leysinger Vieli et al., 2007, 2011).

Here we provide a spatially extensive IRH data set (Cavitte et al., 2020), centered on the Dome C region of the central East Antarctic Plateau. The ages of the IRHs are established using the AICC2012 chronology (Bazin et al., 2013; Veres et al., 2013).

50   The radar transects were collected over a period of 10 years, by several institutes and under the umbrella of numerous projects.

[1].1   The Dome C Plateau region

The Dome C region is a topographic high ($\sim$ 3233 m.a.s.l.) in the interior of the East Antarctic Plateau at the intersection of multiple ice divides (Fig. 1), and in particular the ice divide separating the Byrd Glacier and the Totten Glacier catchments. The ice surface topography is gentle with a change in elevation of $\sim$10 m every 50 km (Genthon et al., 2016). A saddle connects

55   Dome C to Lake Vostok further south along the ice divide. A secondary dome is present $\sim$30 km south of Dome C, referred to as Little Dome C (LDC). The ice flow speed in the region is very low, a few mm yr^{-1} at Dome C, up to $\sim$ 0.21 m yr^{-1} 25 km from the summit (Vittuari et al., 2004). Surface temperatures are very low, reaching $\sim$ -54.5°C on average year-round (EPICA [2]ommmunity members (participants are listed alphabetically) Augustin et al., 2004). The bedrock topography in the Dome C region on the other hand is quite rough. A large subglacial massif is located just a few kilometers south of LDC, where the radar

60   lines are the densest on Fig. 1, and bounded to the north-east by the deep Concordia Subglacial Trench and to the south-west by the Aurora Subglacial Basin (Young et al., 2017). The Concordia Subglacial Trench is itself bounded to the north-east by a 2000 m cliff, the Concordia Ridge. The LDC area was first highlighted as a key Beyond EPICA - Oldest Ice target site in the Van Liefferinge and Pattyn (2013) study. The ice core drilling site has since then been narrowed down to a precise location on LDC through successive radar survey collections (Young et al., 2017) and modeling efforts (Parrenin et al., 2017; Cavitte et al.,

65   2018; Van Liefferinge et al., 2018; Passalacqua et al., 2018), in [3]reparation for drilling (Fig 1).

2   Data and methods

2.1   Ice-penetrating radar systems

The IRHs were traced across multiple ice-penetrating radar surveys that deployed several generations of modern ice-penetrating radar sounders over a decade, between 2008 and 2018, over the Dome C region (Fig.1). The primary set was collected by the

70   University of Texas at Austin Institute for Geophysics (UTIG) and the Australian Antarctic Division (AAD) as part of the ICECAP project (International Collaborative Exploration of the Cryosphere through Airborne Profiling, Cavitte et al., 2016) between 2008 and 2015. This included the Oldest Ice candidate A (OIA) survey flown by ICECAP in January 2016 (Young et al., 2017). Data were collected with the High Capacity Airborne Radar Sounder (HiCARS) 1 & 2 and its Multifrequency Airborne Radar-sounder for Full-phase Assessment (MARFA) descendant; in this paper we refer to these data as HiCARS.

75   The ski-equipped DC-3T Basler was able to operate from Concordia Station, allowing for significant local coverage. The
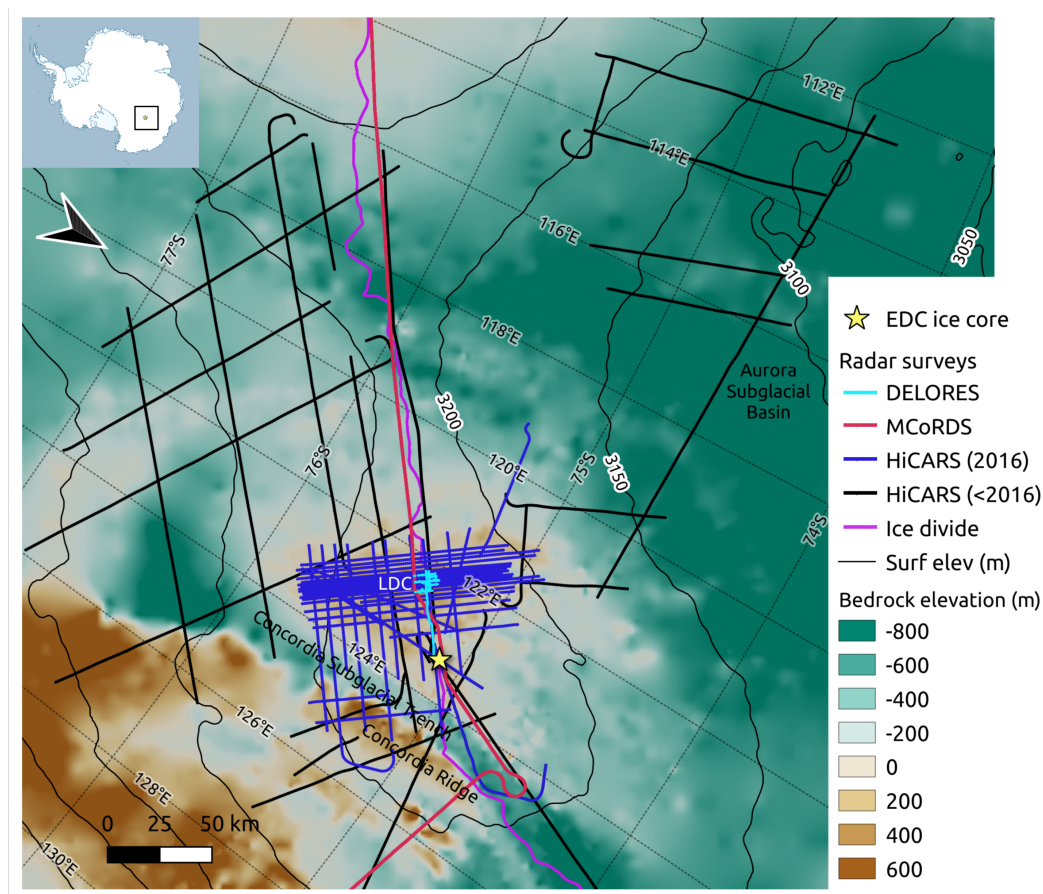
Page: 3

Figure 1. The Dome C region of the East Antarctic plateau with the extent of the ice-penetrating radar surveys used to trace the IRHs, shown as solid lines whose color is a function of the radar system. Background is BedMachine Antarctica v1 bedrock topography (Morlighem et al., 2020) with superimposed CryoSat-2 elevation contours (Helm et al., 2014), a yellow star locates the EDC ice core site, a magenta line locates the Zwally et al. (2012) ice divide in the region, and the main geographical sites are labeled. The inset locates the study area.

Vostok-Dome C airborne radar transect was flown by the Center for Remote Sensing of Ice Sheets (CReSIS) at the University of Kansas using the Multi-Channel Coherent Radar Depth Sounder (MCoRDS) in a single flight line in 2013. A P-3 Orion operating from McMurdo Station collected these data as part of NASA Operation Ice Bridge. We also use a subset of the LDC ground-based radar survey, towed behind a PistenBully PB300 tractor, collected by the Beyond EPICA - Oldest Ice (BE-
80   OI) European Consortium using the British Antarctic Survey's (BAS) Deep Looking Radio Echo Sounder (DELORES) radar system (King et al., 2009).

The main characteristics of each radar system are listed in Tables 2.1 and 2.3. The two fast moving airborne systems improve the Signal to Noise Ratio (SNR) of returning echoes by using long frequency-swept chirp waveforms that are pulse compressed to narrow pulses. Of these two systems, HiCARS has the lowest frequency (60 MHz) and largest compressed pulse

Number: 1 Author: oeisen   Subject: Hervorheben   Date: 29.01.21, 17:38:54
MCoRDS - specify which version

Number: 2 Author: oeisen   Subject: Hervorheben   Date: 29.01.21, 17:41:36
section 2.2.

2.2.3 is just DELORES

Table 1. Ice-penetrating radar system characteristics before focusing and migration.

	HiCARS	MCoRDS	DELORES
Platform	DC-3T Basler	P-3 Orion	PB300 Polar
Source waveform	chirp	chirp	impulse
Frequency range	52.5-67.5 MHz	180-210 MHz	[1]6-7 MHz
PRF	6.4 kHz	12 kHz	1 kHz
Pulse duration	1 μs	1, 3 & 10 μs	0.5 μs
[2]Onboard Presumming	32x	2x, 2x & 32x	1024x
Platform speed	90 m s^{-1}	143 m s^{-1}	3.3 m s^{-1}
Wavelength in air	5.00 m	1.54 m	78.95 m
Along-track sampling[1]	1 m	0.4 m	3 m
Reference	Peters et al. (2005)	Arnold et al. (2020); Rodríguez-Morales et al. (2014); CReSIS (2016)	King (2020)

85 width (100 ns). HiCARS' comparatively low frequency limits surface scattering losses but limits the along-track resolution that can be obtained after post-processing.

The ground based DELORES system uses a broadband impulse and improves SNR by moving slowly along the survey with a high pulse repetition frequency. Scattering losses are avoided by directly coupling the antenna to the surface. The ground based nature of the survey allowed for very tight line spacing to be achieved, however, the area of coverage was limited compared to

90 the airborne surveys.

2.2 Data processing

Data processing must be considered from the perspective of the radar system used and the properties of the targets to be imaged. A key tool is the use of Synthetic Aperture Radar (SAR), which coherently combines echoes over an extended along track distance (the "aperture") to correctly image sloping interfaces and cancel out scattered energy. Processing algorithms for

95 ice are often optimized for the bed, which tends to be rough and scatter diffusively.

The IRHs tend to be distributed specular targets, which means that approaches designed to image the scattering bed are not necessarily appropriate for specular IRHs. In particular, the detected energy from a specular target will be limited to the coherent Fresnel zone, while the range of observable IRH slopes will be a function of the effective beam width derived from SAR processing (Holschuh et al., 2014). Both airborne datasets are visualized in logarithmic power space, with waveform

100 phase removed due to the multilooking (incoherent averaging); the DELORES data are visualized on a relative voltage scale with the positive and negative phase couplets intact. Post-processing data product properties are listed in Table [3]2.3.

---

[1](Holschuh et al., 2014)

5

Page: 5

2.2.1 HiCARS

The balance of coherent versus incoherent stacking, and migration applied in the processing sequence for each radar transect changes for the three types of processing outputs: (1) unfocused SAR ("pik1"), 1-D focused SAR ("foc1") and 2-D focused
105 SAR ("foc2"). In all cases, we range compress and filter the data to obtain vertical pulse widths of 100 ns.

For pik1 we coherently sum the data over 10 records for limited unfocused SAR to derive an effective 3 dB along track beam width of ± 16 degrees. We then incoherently sum the magnitude of the data five times to reduce coherent speckle. This type of processing preserves subsurface energy at the expense of geometric accuracy (Fig. 2) and was used for Cavitte et al. (2016).

To improve along track geometries, we use the matched filter focusing approach of Peters et al. (2007). We first interpolate
110 the data to 1 meter records along track and filter out coherent noise. For foc1, we use focused SAR over the pulse limited footprint ('1-D focusing') to correct for sub vertical resolution range variations (delay changes of 100 ns) that change the phase of individual echoes over synthetic apertures of a few hundred meters. This processing results in improved SNR for rough targets, but causes loss of subsurface IRHs with slopes > 5° (and lower with depth) (Peters et al., 2007). The foc1 processor often produces good results for the bed (particularly in the presence of surface scattering) but is not appropriate for deep IRH
115 tracing (Holschuh et al., 2014).

Our primary processing approach for IRHs was foc2 ('2-D focusing'), where we accommodate range variation of up to 1 μs, allowing our matched filter to track echoes for each point for synthetic apertures of over 2 kilometers. By doing so, IRHs with slopes up to 10° can be detected at depth. This processing comes at the expense of increased noise, and requires more accurate platform position information (which are sometimes unavailable) and computer time. However, we have found foc2
120 to be vital for tracking deep IRHs (Fig. 2). Focused SAR is therefore most useful when reflector geometries are complex (e.g. steep slopes), while pik1 is better suited to relatively smooth internal stratigraphy as it has the highest SNR of all processing products. The resulting post-processed radar data characteristics are listed in Table.2.2.3.

The IRH data set presented here has been traced using the pik1 unfocused SAR and foc2 2-D focused SAR products. The two processing types do not differ much in the Dome C region, due to the exceptionally continuous and relatively flat internal
125 stratigraphy. The biggest differences arise in areas where the IRHs are steeply dipping (Fig.2), as described by Peters et al. (2007). The here published IRH data set therefore clearly states which processing was applied on the radar transect for the IRH interpretation.

2.2.2 MCoRDS

IRHs were traced on the L1B CSARP-standard product. Processing steps involved in creating the L1B CSARP-standard prod-
130 uct are pulse-compression in the frequency domain, with a 20% Tukey window applied in the time domain and a Hanning window applied in the frequency domain, uniform resampling of the data, motion compensation, and finally SAR processing. The SAR processing uses f-k migration with an along-track wavenumber domain Hanning window. The multiple receiver channels are individually SAR processed and then averaged together coherently. Finally, a single image is created by combining the echograms from low (1 μs pulse duration) and high (3 μs and 10 μs pulse duration) gain channels. The effective along track

Number: 1 Author: oeisen　　Subject: Hervorheben　　Date: 29.01.21, 17:50:02
for better readibility, I suggest to use italic pik1, foc1, foc2 throughout the manuscript

Number: 2 Author: oeisen　　Subject: Hervorheben　　Date: 29.01.21, 17:48:49
lengths

Number: 3 Author: oeisen　　Subject: Hervorheben　　Date: 29.01.21, 17:48:59
\circ instead of o

Number: 4 Author: oeisen　　Subject: Hervorheben　　Date: 29.01.21, 17:53:45
\circ

Number: 5 Author: oeisen　　Subject: Hervorheben　　Date: 29.01.21, 17:53:28
fix ref

Number: 6 Author: oeisen　　Subject: Hervorheben　　Date: 29.01.21, 17:51:57
Fig. 2

Number: 7 Author: oeisen　　Subject: Hervorheben　　Date: 29.01.21, 17:52:28
include reference

Table 2. Ice-penetrating radar post-processed data characteristics. Vertical precision is provided for an IRH with 6 dB SNR; Fresnel zone diameter and along track resolution (after focusing and multi-looking) are calculated at 1000 m depth in ice and an altitude of 500 m above the ice in the case of HiCARS and MCoRDS.

	HiCARS (foc2)	MCoRDS (migrated)	DELORES (migrated)
Effective pulse length	100 ns (3 dB point)	51 ns	156 ns
PRF	4 Hz	5 Hz	1 Hz
Vertical resolution in ice	8.42 m	4.30 m	11.09 m
Vertical precision in ice	4.22 m	1.00 m	3.00 m
long-track sampling[1]	21.25 m	30 m	5 m
resnel zone diameter[2]	92.16 m	57.16 m	15.68 m
Along-track resolution	44 m	55 m	22.17 m
Steepest IRH slope	$\pm 10°$	$\pm 5°$	$> \pm 10°$
References	Young et al. (2011); Cavitte et al. (2016)	Arnold et al. (2020); Rodríguez-Morales et al. (2014); CReSIS (2016)	King (2020); Lindsey (1989)

135 beam width is $\pm 5°$ in ice, which limits the detection of IRH with a dip greater than $5°$. The resulting post-processed radar data characteristics are listed in Table 2.2.3 (Arnold et al., 2020; CReSIS, 2016).

2.2.3 DELORES

After GPS-based precise positioning of the raw DELORES radar data, transects are processed using ReflexW (Sandmeier Geophysics) software. Several filters are applied, in the time and depth domains, to increase the SNR of the IRHs, including
140 suppression of the direct air wave, bandpass filtering, a gain function to correct for spherical spreading loss and migration to collapse diffractions to their source points. The original sampling period of 4 ns is averaged to 12 ns in the post-processed data. Because the collection of ground-based radar data is dependent on the speed of the vehicle, which varies due to the terrain roughness during collection, the radar data are interpolated onto a 5 m regular horizontal spacing during post-processing. The resulting post-processed radar data characteristics are listed in Table 2.2.3. The absence of refraction through the air-ice
145 interface allows for very steep IRH slopes to be imaged.

8

Number: 1 Author: oeisen   Subject: Hervorheben   Date: 29.01.21, 18:15:08

Along-track sampling1

where is footnote 1?

Number: 2 Author: oeisen   Subject: Hervorheben   Date: 29.01.21, 18:14:57

Fresnel zone diameter2

where is footnote 2?

Number: 3 Author: oeisen   Subject: Hervorheben   Date: 01.02.21, 09:00:57

2.2.3

2.3 Internal Reflecting Horizons (IRHs)

IRHs are interpreted using Landmark's Decision Space Desktop 5000.8.3.0 software. All the radar transects are loaded into the software prior to interpretation and the built-in basemap is used to track the same IRH continuously from one transect to the next through the use of crossover points (Fig. 3). Prior to loading, the radar transects are flattened to the surface, which is itself

150 set at zero two-way travel time (twtt) so that surface echos and internal stratigraphy match between systems and IRHs can be reliably traced across cross-cutting transects. At each cross over point, the software indicates the twtt of the IRH traced while the 2D viewer allows the visualization of the intersecting radar transects side-by-side to ensure the traced IRH is continuous across the intersection.

To trace the IRHs, we use Decision Space Desktop's semi-automated tracking algorithm to track peaks in the radargram echo
155 amplitudes. This algorithm has a travel-time adjustable window that can be adjusted as a function of the local SNR around the specific IRH being traced. Traced IRHs are chosen based on their brightness and continuity. A traced IRH can start off looking bright and easy to follow, but due to processes such as wind redistribution of surface snow, can get truncated further along a survey transect. Such IRHs are abandoned and only those that could cover > 50% of the whole Dome C region were retained and published in this data set. For HiCARS transects, the type of processing applied (pik1 or foc2) affects the geometry of the
160 IRH. If both types of processing are available for the same transect (this is especially the case for the OIA survey), the IRH is traced separately both in pik1, and in foc2 and each version is then considered as a separate data set.

The dense coverage of the ice-penetrating radar data in the Dome C region means that all radar transects used are directly connected at multiple crossovers. This implies that IRHs can be reliably extended across the whole region by transferring from one profile to the next using matching twtt at the crossover points. This also allows us to perform a check on the IRH tracing,
165 and confirm the isochroneity of the chosen IRHs (see Sect. 4).

2.4 IRH depth and age attribution

2.4.1 Depth attribution

IRHs are traced across all the radar surveys in the Dome C region. The deepest IRHs are truncated on a few radar transects that were flown over steep bedrock topography. This geometry creates steeply dipping IRHs which are difficult to recover in
170 the post-processed data. One of the HiCARS survey lines (MCM/JKB1a/EDMC01a) passes very close to the EPICA Dome C

---

[6] of the final data product

[2] For a chirped system, the Fresnel zone diameter is calculated according to Haynes (2020, Equation S.153):

$$F_s = 2 \sqrt{\frac{C_{air}}{2f_c}(h + \frac{z}{n})} \qquad (1)$$

For a signed waveform system, the Fresnel zone diameter is calculated according to Lindsey (1989):

$$F_s = \frac{C_{ice}}{2f_c\sqrt{2\epsilon'}} \qquad (2)$$

Note that C_{air} is the wave speed in air (3 m s^{-1}), f_c is the center frequency of the radar system, h is the height of the aircraft above the ice, z the depth of interest, $twtt$ is the two-way travel time to the depth of interest, n is the index of refraction of ice (1.78) and ϵ' is the electric permittivity of ice (3.17).

Number: 1 Author: oeisen   Subject: Durchstreichen   Date: 01.02.21, 09:01:29
the

Number: 2 Author: oeisen   Subject: Notiz   Date: 01.02.21, 09:03:28
Does that mean lower SNR = larger window? What does that information help here, how did you use it?

Number: 3 Author: oeisen   Subject: Hervorheben   Date: 01.02.21, 09:05:18
reads as if the wind redistribution acts on deep horizons. Clarify.
Moreover, does the process matter which influences the quality of the horizon? Only the fact counts that it cannot be traced at some point.

Number: 4 Author: oeisen   Subject: Eingefügter Text   Date: 01.02.21, 09:05:41
are

Number: 5 Author: oeisen   Subject: Notiz   Date: 01.02.21, 09:21:56
Footnotes belong to the table. Consider to change footnotes to table comments, which apprear directly underneath the table - makes it more easily understandable.

Number: 6 Author: oeisen   Subject: Hervorheben   Date: 01.02.21, 09:08:10
1of

Number: 7 Author: oeisen   Subject: Hervorheben   Date: 01.02.21, 09:22:25
don't use multiplication signs unless it is a particular mulitiplication (e.g matrix).

Number: 8 Author: oeisen   Subject: Hervorheben   Date: 01.02.21, 09:08:48
No programming slang in a manuscript. Change.

Number: 9 Author: oeisen   Subject: Hervorheben   Date: 01.02.21, 09:09:06
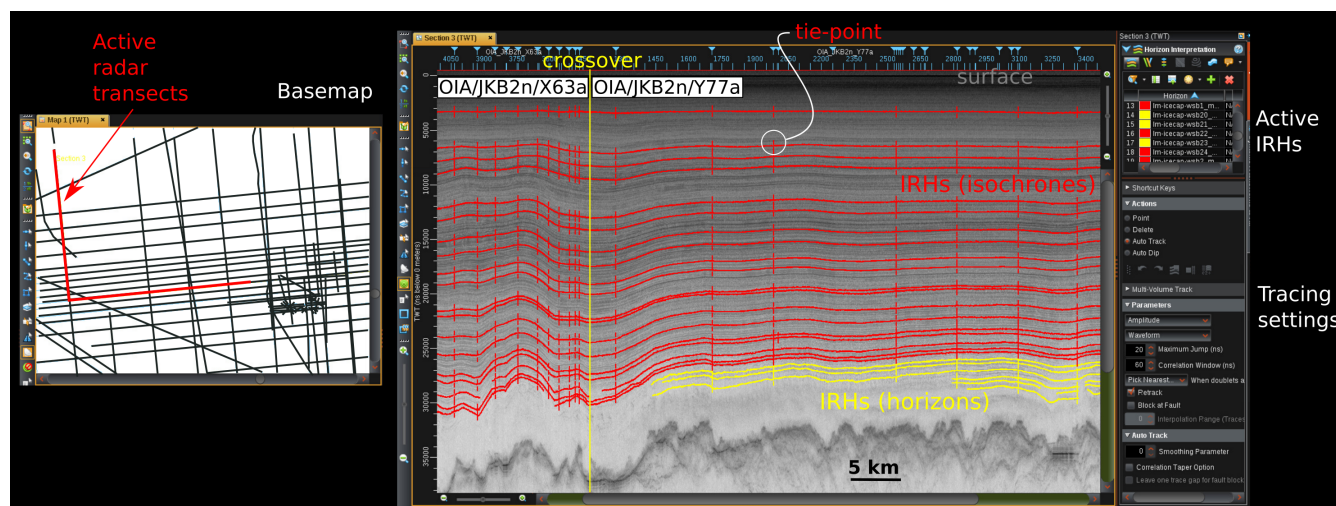relative dielectric permittivity

Figure 3. Screenshot view of the Landmark's Decision Space Desktop software tracing environment. On the right, the 2D section viewer with two radar transects shown and their crossover point indicated by a yellow vertical line. Small ticks indicate the depth of the IRH being traced on a crossing transect, which help ensure the IRHs match up at all crossovers. Red and yellow lines highlight the dated and undated IRHs respectively (see Sect. 2.4.2 for definitions). On the left, the 2D map viewer where the radar transects to be traced can be selected.

(EDC) ice core site (Fig. 1), with a gap of 94 m between the ice core site and the point of closest approach. At this point, the IRH depths can be calculated from their twtt according to the following equation (e.g. Steinhage et al., 2001; MacGregor et al., 2015; Cavitte et al., 2016; Winter et al., 2019):

$$z_{IRH} = \frac{t_{IRH} C_{air}}{2\sqrt{\epsilon'_{ice}}} + z_f \tag{3}$$

175   where the electromagnetic velocity in air (C_{air}) is 300 m μs^{-1}, ϵ'_{ice} is the ice dielectric constant, and z_f is the firn correction. We use an ϵ'_{ice} value of 3.17 (Gudmandsen, 1971; Peters et al., 2005) and a firn correction of 14.60 m following Cavitte et al. (2016), calculated from Eq. 4 in Dowdeswell and Evans (2004) and the Barnes et al. (2002) EDC density profile. Since all our IRHs are below the firn transition, we can ignore variations in ϵ'_{ice} with depth and use a constant value. However, variations in ϵ'_{ice} are taken into account to quantify the IRH depth uncertainties (see Sect. 2.5 below).

180   **2.4.2   Age attribution**

Using the IRH depths measured at the closest point to the ice core site, we can assign ages to the IRHs using the AICC2012 chronology (Bazin et al., 2013; Veres et al., 2013). We linearly interpolate the age-depth chronology to match our IRH depths and date the IRHs. Hereinafter, we refer to these as the "dated IRHs". Note that we use a deterministic approach to date the IRHs, however a Bayesian approach, such as used in Muldoon et al. (2018), could be applied equally to the IRH data. IRHs

185   that cannot be traced all the way to radar transect ICM/JKB1a/EDMC01a, due to stratigraphic discontinuity or radar image quality issues, remain undated. We refer to these IRHs explicitly as "undated IRHs". As a result of their isochronal nature,

Page: 10

these undated IRHs represent informative stratigraphic constraints that can be useful in modelling efforts, and we therefore include them in this data release.

2.5 IRH uncertainty quantification

2.5.1 Depth uncertainties

Cavitte et al. (2016) lists the three main sources of depth uncertainty for IRHs.

First, the vertical resolution of the radar system used, provided in Table 2.3 for each radar system. For chirp systems, by definition, range resolution Δr is given by $\Delta r = C_{ice}/(2 B)$, where B is the bandwidth of the radar system, or equally $\Delta r = (C_{ice} \, pw)/2$ where pw is the effective pulse duration. In the case of the CReSIS system, because of the 20% Tukey time-domain window and Hanning frequency-domain window applied, range resolution is given by CReSIS (2016) as $\Delta r = (k_t \, C_{ice})/(2 B)$, where $k_t = 1.53$ is the window widening factor computed numerically to find the pulse width 3 dB down from the peak. For a signed, low frequency, waveform, as found in DELORES radargrams, the above rule does not apply, and for range resolution we instead use: $\Delta r = \lambda_{ice}/4$, where λ is the wavelength of the signal in ice. Following Cavitte et al. (2016), since we are interested in identifying individual specular returns in the ice, by measuring the SNR of each IRH at the ice core site, we can calculate the range precision, $\sigma(r*)$ of each IRH according to:

$$\sigma(r) = \frac{\Delta r}{SNR}$$

(4)

Range precision is improved over range resolution for an IRH SNR greater than one. Note that the range precision calculated is valid at the EDC site, but might not be constant laterally, since IRH SNR varies spatially. However, we assume it provides a representative value of the "real" $\sigma(r*)$ value for each IRH. This range precision calculation assumes a single resolved target, and the precision could be worse if two or more IRHs of comparable power are present.

A second source of uncertainty comes from measurement errors in the depth-density curves used to calculate the firn correction. We use a depth error of $\pm$ 1.35 m at the EDC site as described in Cavitte et al. (2016), based on the Barnes et al. (2002) published measurement errors.

A third source of uncertainty comes from the variations in the dielectric constant, as a function of temperature, impurity concentration and anisotropy (Peters et al., 2005; Fujita et al., 2000), which affects the calculated IRH depths. Electromagnetic velocities in ice vary between 168 and 169.5 m μs^{-1} (Fujita et al., 2000), which increases the uncertainty in the depth calculations with depth. For the deepest dated IRH traced (366 ka), this represents a maximum depth error of $\pm$ 11.65 m at the EDC site.

The total depth uncertainty is the root-sum-square error of each of these three uncertainties. It is calculated for each dated IRH and listed in Table 5.1.

Additional, but not quantified, sources of uncertainty come from (1) the assumption of horizontal continuity of the IRHs between the EDC site and the radar transect, which corresponds to a distance of $\sim$ 94 m; (2) the complexity of tracing the same IRH across two radar transects from different systems (discussed in Sect. 4); (3) vertical advection over the 10 years of data

11

Number: 1 Author: oeisen Subject: Notiz Date: 01.02.21, 09:21:30
no new paragraph

Number: 2 Author: oeisen Subject: Notiz Date: 01.02.21, 09:24:14
Grammar seems wrong in this sentence

Number: 3 Author: oeisen Subject: Hervorheben Date: 01.02.21, 09:21:33
2.2.3

Number: 4 Author: oeisen Subject: Durchstreichen Date: 01.02.21, 09:23:38

Number: 5 Author: oeisen Subject: Notiz Date: 01.02.21, 09:24:55
again I suggest to switch to a single-letter variable, e.g. p_w

Number: 6 Author: oeisen Subject: Durchstreichen Date: 01.02.21, 09:23:44

Number: 7 Author: oeisen Subject: Durchstreichen Date: 01.02.21, 09:23:49

Number: 8 Author: oeisen Subject: Durchstreichen Date: 01.02.21, 09:23:53

Number: 9 Author: oeisen Subject: Notiz Date: 01.02.21, 09:27:15
you could express lambda directly here as a function of c and frequency, as you only provide those in the table.
You could also consider to add lambda_ice in the table in addition to lambda_air (as ice is more relevant).

Number: 10 Author: oeisen Subject: Hervorheben Date: 01.02.21, 09:28:02
what the * symbol now? Multiplication, as you used it above?

Number: 11 Author: oeisen Subject: Hervorheben Date: 01.02.21, 09:28:15
see line above

Number: 12 Author: oeisen Subject: Hervorheben Date: 01.02.21, 09:29:22
For this equation to make sense SNR is given in a linear scale; or is it dB or something else? Clarify.

Number: 13 Author: oeisen Subject: Eingefügter Text Date: 01.02.21, 09:29:38
.

Number: 14 Author: oeisen Subject: Hervorheben Date: 01.02.21, 09:30:00
IRH with a SNR >1

Number: 15 Author: oeisen Subject: Eingefügter Text Date: 01.02.21, 09:31:14
permittivity

Number: 16 Author: oeisen Subject: Hervorheben Date: 01.02.21, 09:32:01
3 it should be?

Table 3. Depths, ages and uncertainties of the 19 dated IRHs, measured and calculated at the EDC site, using the AICC2012 chronology (Bazin et al., 2013; Veres et al., 2013). Δz and Δa stand for depth and age uncertainty, respectively.

Dated IRH	depth (m)	age (ka)	Δz (m)	Δa (kyr)
OIA_EDC_IRH1	308.20	9.99	3.17	0.28
OIA_EDC_IRH2	602.60	29.38	3.74	0.90
OIA_EDC_IRH3	699.60	38.11	3.96	0.67
OIA_EDC_IRH4	798.60	46.41	4.01	0.86
OIA_EDC_IRH5	1076.10	73.37	5.38	2.12
OIA_EDC_IRH6	1171.90	82.01	5.51	1.59
OIA_EDC_IRH7	1337.90	96.49	6.55	1.80
OIA_EDC_IRH8	1446.80	106.25	6.88	1.91
OIA_EDC_IRH9	1593.90	121.09	7.48	1.77
OIA_EDC_IRH10	1682.10	127.78	7.81	1.84
OIA_EDC_IRH11	1888.40	160.37	8.79	3.91
OIA_EDC_IRH12	1917.10	166.35	9.14	3.59
OIA_EDC_IRH13	2076.20	200.12	9.66	2.63
OIA_EDC_IRH14	2193.40	220.06	10.07	3.34
OIA_EDC_IRH15	2336.80	254.46	12.59	5.47
OIA_EDC_IRH16	2402.30	277.90	11.15	4.89
OIA_EDC_IRH17	2543.70	327.34	11.77	4.11
OIA_EDC_IRH18	2598.20	341.48	11.70	5.59
OIA_EDC_IRH19	2644.30	366.49	12.08	7.90

Note that values have been updated since Cavitte et al. (2016).

collection, although, considering the radar resolutions and the surface accumulation rate, this (3) can be neglected; and (4) the assumption that only a single target is present in the range precision estimate for the IRH.

Depth uncertainties are also assigned to the undated IRHs (Table 3). Since these IRHs do not reach the MCM/JKB1a/EDMC01a transect, their depths are measured at the closest point along the DELORES radar transect HRB7-HRB8 to the final chosen E-OI drill site (75.29917°S, 122.44516°E), and their uncertainties are constrained as described above but with their range precision defined by their SNR along this DELORES transect. We assume that the firn correction and error calculated at the EDC site are also applicable to this site over LDC.

2.5.2 Age uncertainties

The total age uncertainty of an IRH results from the combination of the published ice core age uncertainty, $\Delta a_{\Delta core}$ (Bazin et al., 2013; Veres et al., 2013) and the IRH's depth uncertainty, $\Delta a_{\Delta z}$ (described above). The depth uncertainty is converted to

Number: 1 Author: oeisen   Subject: Durchstreichen   Date: 01.02.21, 09:33:10

Number: 2 Author: oeisen   Subject: Durchstreichen   Date: 01.02.21, 09:33:13

Number: 3 Author: oeisen   Subject: Hervorheben   Date: 01.02.21, 09:35:01
cosider to mention both values here again so that the reader get's that right away without having to look it up again.

Number: 4 Author: oeisen   Subject: Hervorheben   Date: 01.02.21, 09:34:33
we assume that this factor

Number: 5 Author: oeisen   Subject: Hervorheben   Date: 01.02.21, 09:36:02
the official name of the drill site is BELDC. Please use that throughout the ms.

Number: 6 Author: oeisen   Subject: Hervorheben   Date: 01.02.21, 09:36:27
provide reference to Lilien et al., 2020, TDC .

an age uncertainty using the AICC2012 chronology to calculate the local age gradient for each IRH depth. These two sources

230   of uncertainties are combined as a root-sum-square error as in Cavitte et al. (2016); Winter et al. (2019):

$$\Delta a = \sqrt{\Delta a_{\Delta z}^2 + \Delta a_{\Delta core}^2} \tag{5}$$

Combined age uncertainties (Δa) calculated for each dated IRH are summarized in Table 5.1.

3   Results

In total, 26 IRHs are traced across the wider Dome C region, using the 79 radar transects, representing > 15,500 kilometers

235   of IRH data interpreted over this part of the East Antarctic Plateau (Fig. 1, Cavitte et al., 2020). Of these 26 IRHs, 19 IRHs
are dated. These dated IRHs span four glacial cycles, from the shallowest IRH dated at ∼10 ka to the deepest IRH dated at
∼ 366 ka (Table 5.1 and Fig. 4). Figure 5 shows the depth distribution of all 19 dated IRHs as a percentage depth anomaly
of the IRH from its average depth from the surface of the ice. The LDC is a region where the combination of the very flat
internal stratigraphy (due to the low surface velocities) and very cold ice results in all 19 dated IRHs continuously traced over

240   the whole area. As we step off the LDC bedrock plateau, the deepest IRHs drop off (in particular the bottom three). Affected by
the presence of the deep Concordia Subglacial Trench on the north-east side (∼ 600 m cliff) and the Aurora Subglacial Basin
on the south-west side, the IRHs steepen, with the strongest impact on the deepest ones. We observe a gradient, consistent
for all dated IRHs, of depth shallowing from the north side of Dome C to its south side. This has been observed previously
(Urbini et al., 2008; Verfaillie et al., 2012; Cavitte et al., 2018; Le Meur et al., 2018; Frezzotti et al., 2005) and results from the

245   accumulation gradient at the surface with average moisture provenance from the Indian Ocean moving across the ice divide
(Scarchilli et al., 2011). Although the deepest dated IRH reaches on average 81% of the ice thickness, with local maxima of
∼90%, its age of 366 ka represents only ∼45% of the total age interval measured at EDC.

Of the 26 IRHs traced in the Dome C region, seven IRHs remain undated. The seven undated IRHs are also the deepest IRHs.
The difficulty in connecting them to the MCM/JKB1a/EDMC01a radar transect stems from their proximity to the bedrock

250   which induces strongly dipping internal geometries that become difficult to track continuously. We plot the depth distribution
of all seven undated IRHs (Fig. 6) which are much less extensive than the dated IRHs, and are constrained to the LDC highland
region. We can see that the deepest undated IRH reaches on average ∼89% depth of the ice thickness, with local maxima
reaching 90-92%, relatively close to the bedrock.

We use the 1-D pseudo-steady (Parrenin et al., 2006) ice flow model described in Parrenin et al. (2017) to assign a mean

255   age to the undated IRHs. We use the above (19) dated IRHs as age and depth constraints to calculate a steady state age-depth
modeled field for each radar transect. The ages simulated for the bottom ∼20% of the ice sheet, i.e. older than 366 ka, are
therefore extrapolated ages. From the measured undated IRHs depths, we can then sample the simulated age-depth field and
assign a modeled age to every trace along the radar transects (Fig. 7). We can then calculate a mean modeled age for each
undated IRH, provided in Table 3, as well as the age standard deviation, based on their modeled spatial age distribution. The

260   deepest IRH, with a modeled age of 709 ka, has an average depth of 89% over its whole extent, and reaches 90% of the ice

13

Number: 1 Author: oeisen	Subject: Eingefügter Text	Date: 01.02.21, 09:36:58	

and

Number: 2 Author: oeisen	Subject: Eingefügter Text	Date: 01.02.21, 09:37:04	

.

Number: 3 Author: oeisen	Subject: Hervorheben	Date: 01.02.21, 09:37:17	

3

Number: 4 Author: oeisen	Subject: Hervorheben	Date: 01.02.21, 09:37:50	

km

Number: 5 Author: oeisen	Subject: Hervorheben	Date: 01.02.21, 09:37:41	

kilometers

Number: 6 Author: oeisen	Subject: Hervorheben	Date: 01.02.21, 09:38:09	

2.5.1

Number: 7 Author: oeisen	Subject: Hervorheben	Date: 01.02.21, 09:41:09	

above you mentioned surface redistribution, which does not fit to this statement to maintain layer integrity. Seems a bit inconsistent. Unclear in the text what cold ice has to do with this (and what is very cold ice?Quantify).

Number: 8 Author: oeisen	Subject: Hervorheben	Date: 01.02.21, 09:38:40	

in which direction?

Number: 9 Author: oeisen	Subject: Hervorheben	Date: 01.02.21, 09:41:35	

unclear what you mean

Number: 10	Author: oeisen	Subject: Hervorheben	Date: 01.02.21, 09:44:47

we can then

Number: 11	Author: oeisen	Subject: Hervorheben	Date: 01.02.21, 09:45:51

We can then ...
yes, you can, but if you do it, you should also write
We calculate ... we sample ... etc.

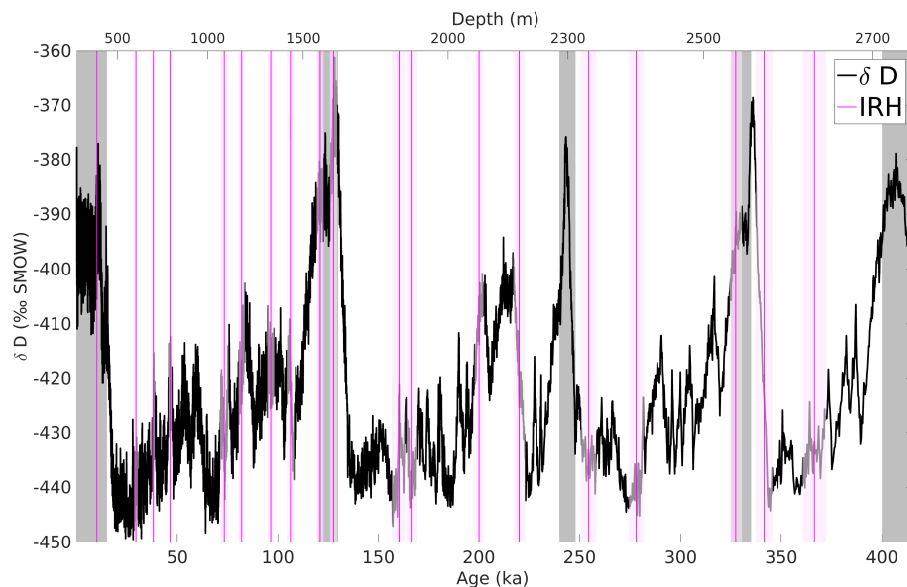|			
Number: 12	Author: oeisen	Subject: Hervorheben	Date: 01.02.21, 09:45:05

then

Figure 4. Temporal coverage of the dated IRHs (marked in magenta) over the past four glacial cycles, here displayed on top of δD variations measured on the EDC ice core and using the AICC2012 chronology (Bazin et al., 2013). IRH age uncertainties are indicated by pink vertical bounds. Interglacials are highlighted in grey.

thickness at the closest point to the final chosen [1]E-OI drill site. This implies a [2]deep age gradient in the bottom ∼10% of the ice locally with strong implications for resolving the climate signal of the deep ice core to be recovered.

[3]Note that there is now evidence that there is a layer of ice just above the bed, and in particular over the LDC highland plateau, with [4]completely different electromagnetic properties, which could be stagnant. The (Parrenin et al., 2017) ice flow

265 model version used does not take this stagnant ice into account, which could make the basal ages, and therefore the seven bottom IRHs, too young in the present modelling. A new version of the 1-D model that takes into account this stagnant layer has been developed and it will be interest to compare the new ages obtained (Fred Parrenin, pers. comm.).

4 Discussion

We were able to map the internal stratigraphy extensively throughout the Dome C plateau region as a result of the good

270 glaciological conditions for ice-penetrating radar imaging: slow ice flow velocities in the region, [5]cold surface temperatures year round and the lack of any (known) history of paleo flow direction switches. All these factors combine to create smooth, continuous and bright IRHs that can be traced over very long distances. Siegert et al. (1998a) was already able to trace IRHs in the vicinity of Dome C without encountering continuity issues. Difficulties mostly arose in approaching the Vostok ice core site some 500 km away due to wind-driven snow redistribution buried beneath the surface, as well as the advected accumulation

275 high over the Vostok Lake (Leonard et al., 2004; Cavitte et al., 2016).

Number: 1 Author: oeisen　　　Subject: Hervorheben　　　Date: 01.02.21, 09:49:38
BELDC

Number: 2 Author: oeisen　　　Subject: Hervorheben　　　Date: 01.02.21, 09:50:10
severe

Number: 3 Author: oeisen　　Subject: Notiz　　Date: 01.02.21, 09:52:09
This parapgraph should go into the discussion, not in your results.

Number: 4 Author: oeisen　　Subject: Hervorheben　　Date: 01.02.21, 09:51:18
we assume so, but we do not know. Rather other dynamic properties. Therefore you should reduce this implications of this statement.
Cite Lilien et al. 2020 TCD, which describe this layer.

Number: 5 Author: oeisen　　Subject: Hervorheben　　Date: 01.02.21, 10:58:05
be more specific! Change to
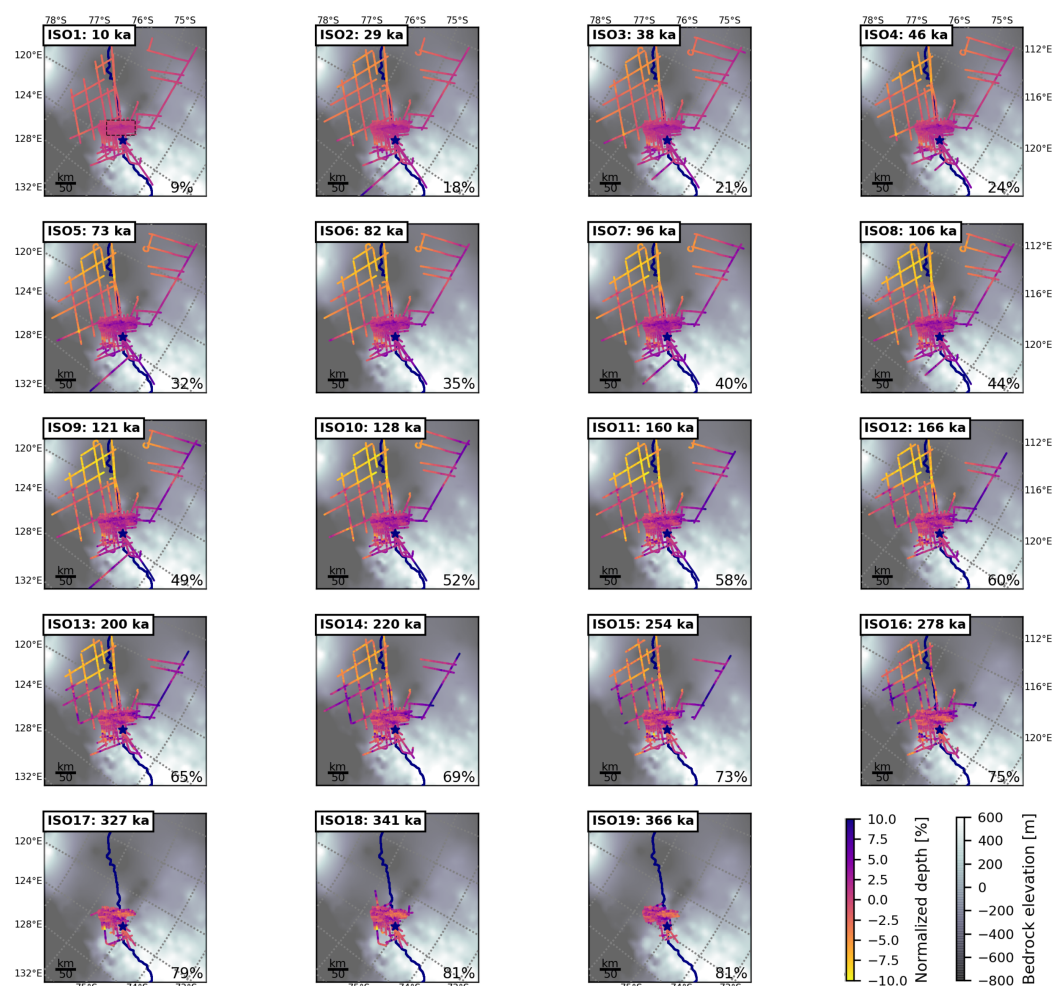"absence of melting at the surface with maximum temperatures not exceeding -15C (citation) ..."

Figure 5. Spatial distribution of dated IRH depths over the Dome C region of the East Antarctic Plateau, overlain on BedMachine Antarctica v1 bedrock topography (Morlighem et al., 2020) for context. The color scale represents the percent depth anomaly of the IRH from its average percent depth (marked in the bottom right corner of each panel): darker colors imply that the IRH is deeper locally than on average, lighter colors imply that the IRH is shallower locally than on average. Percent depths are normalized by the ice thickness, both measured from the radar returns. The navy star locates the EDC ice core site and the navy line outlines the position of the ice divide (Zwally et al., 2012). A black dashed box on the first panel outlines the LDC highland area covered by Figs. 6 and 7.

In the data set published here (Cavitte et al., 2020), we observe no obvious signs of disruptions in the englacial stratigraphy. This is consistent with the Das et al. (2013) distribution of glazed areas and known megadune areas (Frezzotti et al., 2005; Arcone et al., 2012). Most difficulties in tracing IRHs arise for the deepest IRHs. Robin and Millar (1982) first described how the effect of the bedrock topography has the strongest impact on the internal stratigraphy immediately above the bed, and decreases with distance from the bed, while modeling efforts have brought to light the influence of basal processes on internal
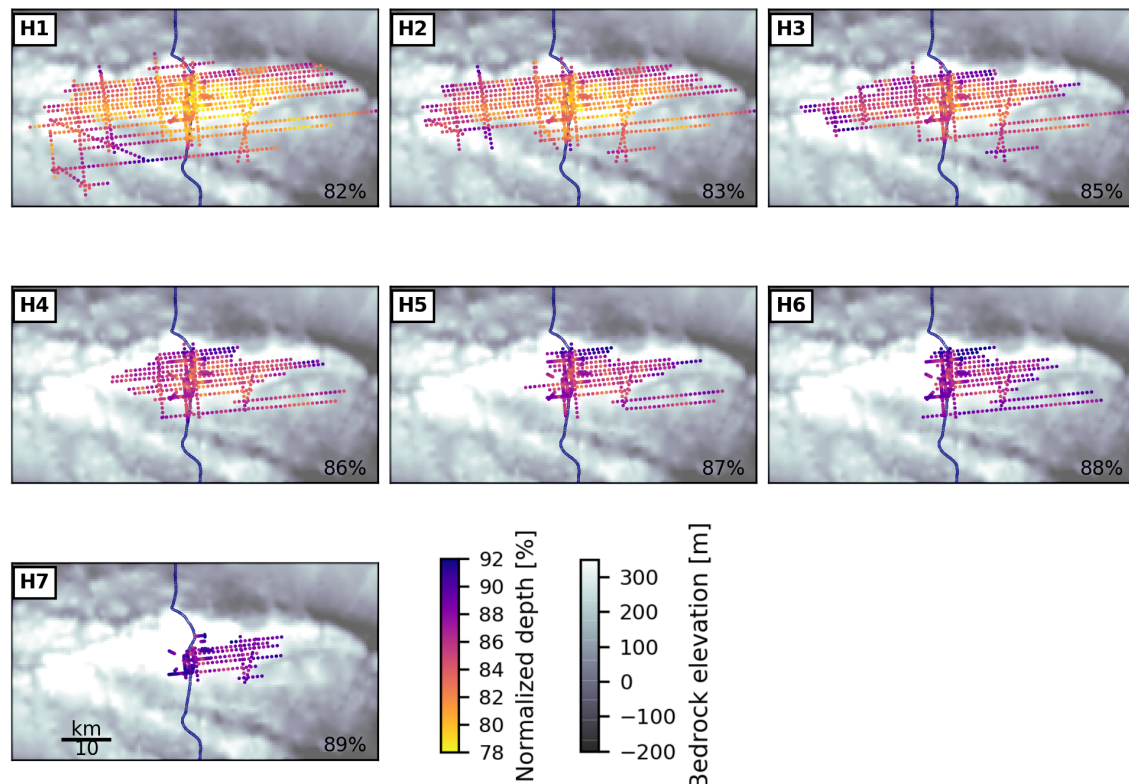
280

15

Page: 15

Figure 6. Spatial distribution of undated IRH depths over the LDC highland plateau on the East Antarctic Plateau, overlain on Young et al. (2017) bed elevations. The area covered by each panel is outlined by a black dashed box on the first panel of Fig. 5. The color scale represents the depth of the IRHs normalized by the ice thickness, both measured from the radar returns. The navy line outlines the position of the ice divide (Zwally et al., 2012).

stratigraphy (Leysinger Vieli et al., 2011; Vieli et al., 2018). This effect is obvious, even visually, in the IRHs presented here (Fig. 3). Because the deepest IRHs are generally the steepest, their coverage is limited (Fig. 7). Holschuh et al. (2014) have shown how the different types of radar processing can create destructive interference in case of steeply dipping surfaces in the along track direction; similarly, steep dips across track can fall into nulls in the across track beam pattern. This is particularly true e.g. across the Concordia Subglacial Trench. Here, the 600 m trench, followed by the 600 m cliff of the Concordia Ridge have a strong effect on the IRH geometries (Parrenin et al., 2017; Passalacqua et al., 2018). Furthermore, the ice becomes warmer the closer it gets to the bed as a result of the thick insulating ice above and the conduction of geothermal heat from below (Pattyn, 2010; Van Liefferinge and Pattyn, 2013). Temperature affects the dielectric permittivity of the ice and can result in a strongly attenuated radar return (Matsuoka, 2011; MacGregor et al., 2012).

Number: 1 Author: oeisen   Subject: Hervorheben   Date: 01.02.21, 09:47:58
Bedrock seems saturated in white, thus losing details. Please adjust the greyscale.

Geographical coordinates required, as in Fig. 5.

Number: 2 Author: oeisen   Subject: Hervorheben   Date: 01.02.21, 09:46:44
navy blue

Number: 3 Author: oeisen   Subject: Hervorheben   Date: 01.02.21, 11:00:59
a competition between decreasing advection from above and increasing conduction ...

Number: 4 Author: oeisen   Subject: Notiz   Date: 01.02.21, 11:01:49
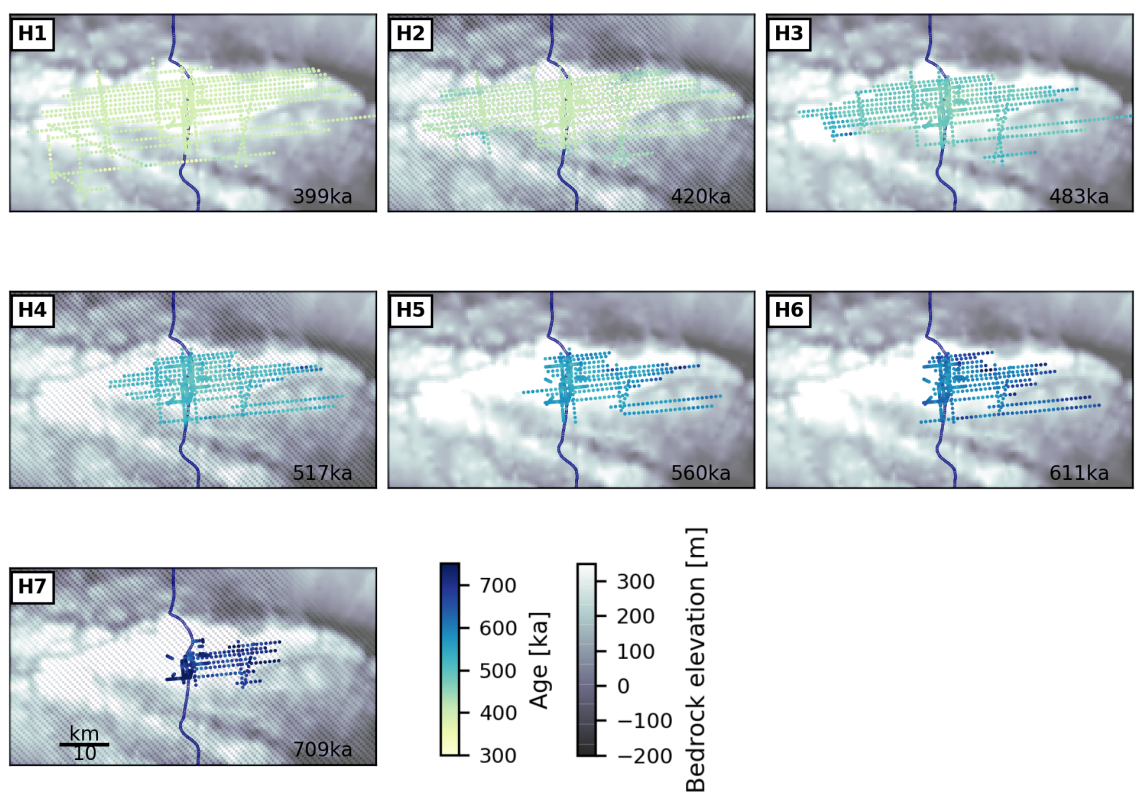So what's the influence on your data here? Reduced SNR?

Figure 7. Spatial distribution of modeled ages for the seven bottom IRHs over the Dome C region of the East Antarctic Plateau, overlain on Young et al. (2017) bed elevations. The area covered by each panel is outlined by a black dashed box on the first panel of Fig. 5. The color scale represents the predicted age of the model-dated IRHs, interpolated from the modeled age-depth field. The navy line outlines the position of the ice divide (Zwally et al., 2012).

290   In using several radar systems, there is the added difficulty of tracing IRHs reliably from one radar system to the next at crossover points (Cavitte et al., 2016; Winter et al., 2019). Cavitte et al. (2016) have shown that transferring IRHs from the HiCARS system to the MCoRDS system is tractable, despite the differences in their range resolutions. Because MCoRDS has a finer range resolution (4.30 m for MCoRDS vs 8.42 m for HiCARS), some of the IRHs selected in the HiCARS radargrams correspond to two IRHs on the MCoRDS radar transect (Fig. 8, panel b). However, Cavitte et al. (2016) show that the IRHs can

295   be traced over 100s of kilometers and still match between the two radar systems within their age uncertainty ranges. Similarly, Winter et al. (2019) show that their IRHs, traced using the Alfred Wegener Institute (AWI) radar system with a pulse source waveform and a range resolution of 5 m, can be matched to the HiCARS IRHs presented in this data release. Similarly, tracing the IRHs across from the airborne-collected HiCARS radar data to the ground-based DELORES radar data is also tractable,

17

Number: 1 Author: oeisen Subject: Hervorheben Date: 01.02.21, 11:04:14
tractable, trackable or traceable?
Up for a native english-speaking coauthor to decide.

Number: 2 Author: oeisen Subject: Eingefügter Text Date: 01.02.21, 11:03:42
60 ns

Table 4. Depths and modeled mean ages for the seven model-dated IRHs, using the Parrenin et al. (2017) 1-D steady-state ice flow model. Depths are measured at the closest point along the DELORES radar transect HRB7-HRB8 to the final ~~BE-OI~~ [1] ll site (measured local ice thickness of ~2747 m), and depth uncertainties are calculated as described in Sect. 2.5 for that same location along transect HRB7-HRB8. Age uncertainties here are mostly representative of the model age uncertainty: they are calculated as the standard deviation of the spatial distribution of the age of each IRH.

Model-dated IRH	depth (m)	mean age (ka)	Δz ($\pm$m)	stdev age ($\pm$kyr)
OIA_EDC_IRH20	2256.27	399.49	13.36	9.65
OIA_EDC_IRH21	2285.13	419.83	13.54	13.66
OIA_EDC_IRH22	2351.45	482.72	13.76	22.07
OIA_EDC_IRH23	2381.81	516.75	14.36	21.92
OIA_EDC_IRH24	2410.52	560.15	13.94	27.24
OIA_EDC_IRH25	2440.06	610.95	14.31	35.44
OIA_EDC_IRH26	2495.86	708.54	13.80	54.01

with a difference in range resolution of 2.85 m (8.42 m versus 11.09 m). Figure 8, panel a, shows a very good one-to-one match in the IRHs. The 26 IRHs can be traced through all of the DELORES radar transects presented here.

[2] will be interesting, and this is the goal of the AntArchitecture community, to have a joint community effort to build an Antarctic-wide IRH data set to check the match between all previously traced and published IRH data sets that can be directly connected for the East Antarctic Plateau region (to name a few, Siegert et al., 1998a; Winter et al., [3] 019), and eventually [4] ~~connecting to~~ IRHs from currently disconnected surveys (e.g. Steinhage et al., 2001; Leysinger Vieli et al., 2011; Steinhage et al., 2013) [5] er the collection of additional radar campaigns in the gap areas. The Greenland Ice Sheet already benefits from an ice sheet-wide IRH data set (MacGregor et al., 2015) and several studies have demonstrated this is achievable for the West Antarctic Ice Sheet (Muldoon, 2018; Ashmore et al., 2020). Efforts are already underway in the modeling community to integrate these data sets which provide previously rare internal tuning constraints, as opposed to the traditionally used surface and basal boundary conditions (Medley et al., 2013; Muldoon, 2018; Sutter et al., 2020).

5 Conclusions

We traced 26 IRHs across the Dome C plateau region, including 19 that could be dated at the EDC site, and another seven undated IRHs, constrained to the LDC highland area. We publish this internal stratigraphy data set ([6] avitte et al., 2020) with the associated depth and age uncertainties of each IRH. The dated IRHs span the last four glacial cycles, the youngest dated at 10±0.25 ka and the oldest dated at 366±5.78 ka. The bottom seven IRHs are provided with ages using a 1-D inverse model, which indicate an oldest predicted age of ~709 ka. In this region of the East Antarctic Plateau, the biggest limitation in the tracing of the deep IRHs is their proximity to the rugged bedrock that induces both dipping geometries as well as attenuated

---

Number: 1 Author: oeisen   Subject: Eingefügter Text   Date: 01.02.21, 11:05:42

BELDC

Number: 2 Author: oeisen   Subject: Hervorheben   Date: 01.02.21, 11:07:57

The formulated goal of the AntArchitecture community is to make a

---

Number: 3 Author: oeisen   Subject: Hervorheben   Date: 01.02.21, 11:08:23

2019). Eventually,

Number: 4 Author: oeisen   Subject: Durchstreichen   Date: 01.02.21, 11:08:30

connecting to

Number: 5 Author: oeisen   Subject: Eingefügter Text   Date: 01.02.21, 11:08:39

should be connected

Number: 6 Author: oeisen   Subject: Eingefügter Text   Date: 01.02.21, 11:09:25
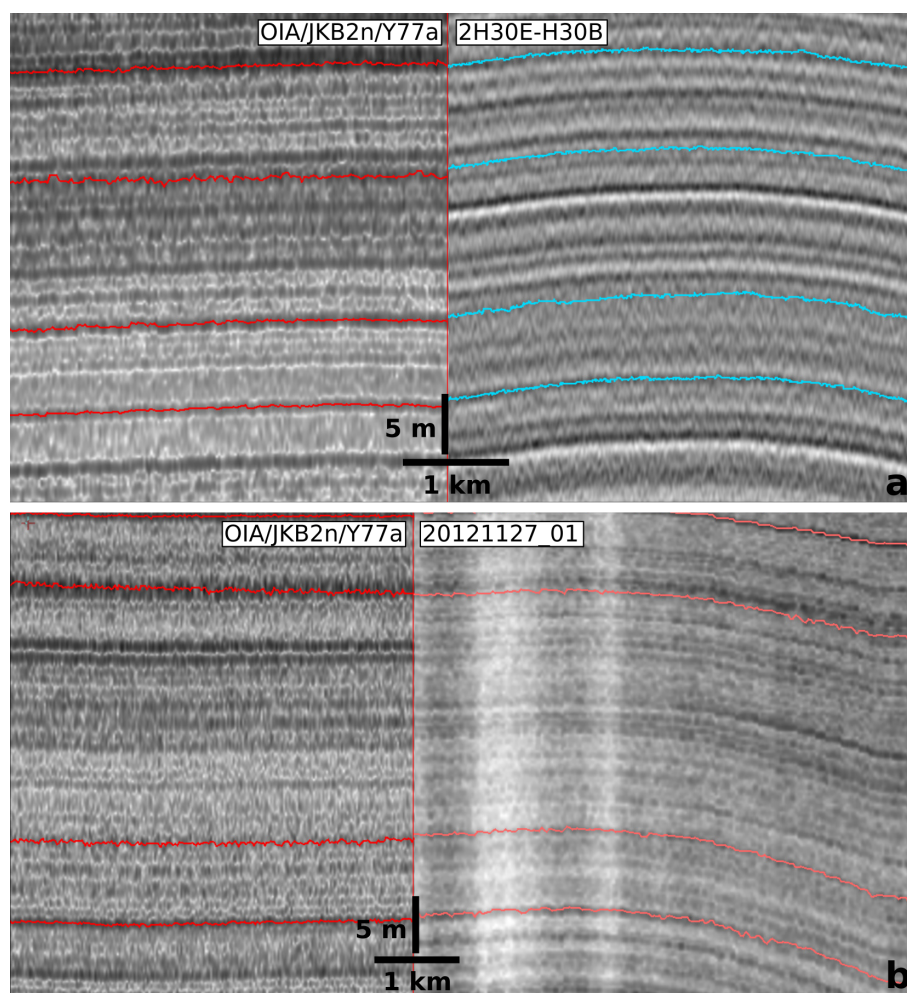
in a long-term data repository

Figure 8. Zoomed-in view of the crossovers and the IRH matches between an OIA transect (OIA/JKB2n/Y77a) and (a) DELORES transect 2H30E-H30B, and (b) MCoRDS transect 20121227_01. Vertical and horizontal scales are provided on each panel.

radar returns due to higher basal ice temperatures. Nevertheless, at the LDC highland region near Dome C, we are able to trace IRHs down to a depth of ∼89% of the ice thickness. These data confirms that 1.5 million-year-old ice will be found in the bottom 10% of the ice sheet (Parrenin et al., 2017).

320 ## 6 Code and data availability

The IRHs presented in this study can be found publicly on the U.S. Antarctic Program Data Center (USAP-DC): https://doi.org/10.15784/601411 (Cavitte et al., 2020). The code for the 1-D steady-state ice flow model is available publicly at https://github.com/parrenin/IsoInv.

Number: 1 Author: oeisen   Subject: Eingefügter Text   Date: 01.02.21, 11:05:24
HiCARS

Number: 2 Author: oeisen   Subject: Eingefügter Text   Date: 01.02.21, 11:10:18
and thus lower SNR.

Number: 3 Author: oeisen   Subject: Hervorheben   Date: 01.02.21, 11:16:53
This statement goes beyond what is necessary in this paper and, in fact, what you showed. That's done by Lilien et al 2020 TCD. Therefore delete this sentence.
Rather you could state that your data set provides the basis for a regional assessment of age at larger depth for other planned deep drillings in this region (e.g. Australia).